ISTITUTO NAZIONALE DI FISICA NUCLEARE
Sezione di Trieste

INFN/TC-02/07
10 aprile 2002

A novel scheme for the integrated voltage divider of Silicon Drift Detectors

P. Burger[1], C. Piemonte[2], A. Rashevsky[3], A. Roncastri[2], A. Vacchi[3]
[1)] *Canberra Semiconductors N.V., Olen, Belgium*
[2)] *Università di Trieste, Dipartimento di Fisica, Via A. Valerio 2, I-34127 Trieste, Italy*
[3)] *INFN, Sezione di Trieste, Via A. Valerio 2, I-34127 Trieste, Italy*

Abstract

Developing a large area silicon drift detector (SDD) for the ALICE experiment, one of the objectives was to work out a robust and redundant design. As soon as the detector is planned to work without an external divider, the integrated voltage divider plays an important role. Unlike the case of silicon microstrip or pixel detectors, a single defect in the SDD may be propagated throughout the whole detector. We report a new design of the integrated voltage divider that allows to prevent this propagation in most practical cases. Device simulations complement laboratory measurements.

Published by **SIS-Pubblicazioni**
Laboratori Nazionali di Frascati

1 Biasing scheme of the ALICE SDD.

Usually, a linear silicon drift detector consists of two symmetrical halves. In each half, on both detector sides, the drift p^+ cathodes are connected in chain via an external or an integrated voltage divider [1-16]. The cathode with the highest negative potential is common for both half-detectors (figure 1). Guard p^+ cathodes, situated at the left and right flanks of the sensitive region, serve to scale gradually the high negative potentials towards the ground potential of the detector edge. A guard connects corresponding drift cathodes of opposite halves (see figure 1). In this way a deviation of the potential distribution of a

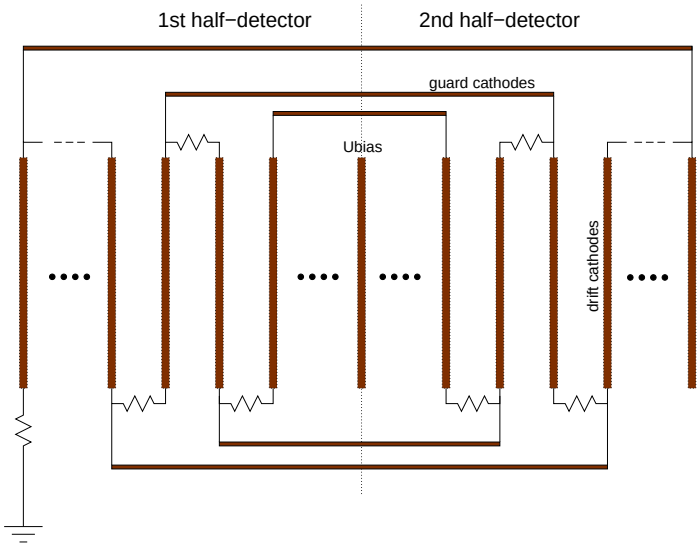

Figure 1: Sketch of the connections between drift and guard cathodes in a standard linear SDD.

half-detector (from the linear one) is completely reproduced on the other half.

To avoid this situation, we implemented a new biasing scheme in which separate dividers bias the drift and guard cathodes. As shown in figures 2 and 3, we provided only a “soft” connection between the structures. Every resistor of the integrated dividers (realised as low doped p^+ implants) is equipped with a MOS switch, as shown in figure 3a. The gate of the MOS is connected to the drift resistor (see figure 3b). The ’soft’ connection between corresponding drift cathodes of opposite halves can be described as ’1st_half_drift_cathode - MOS - guard_cathode - MOS - 2nd_half_drift_cathode’.

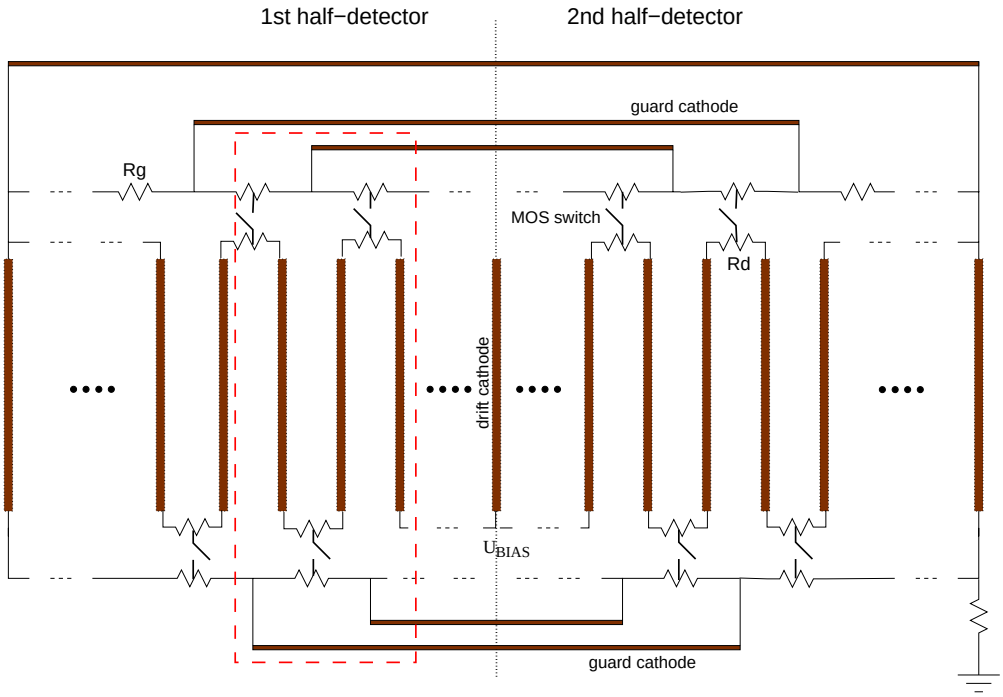

Figure 2: Sketch of the connections between drift and guard cathodes in the ALICE SDD.

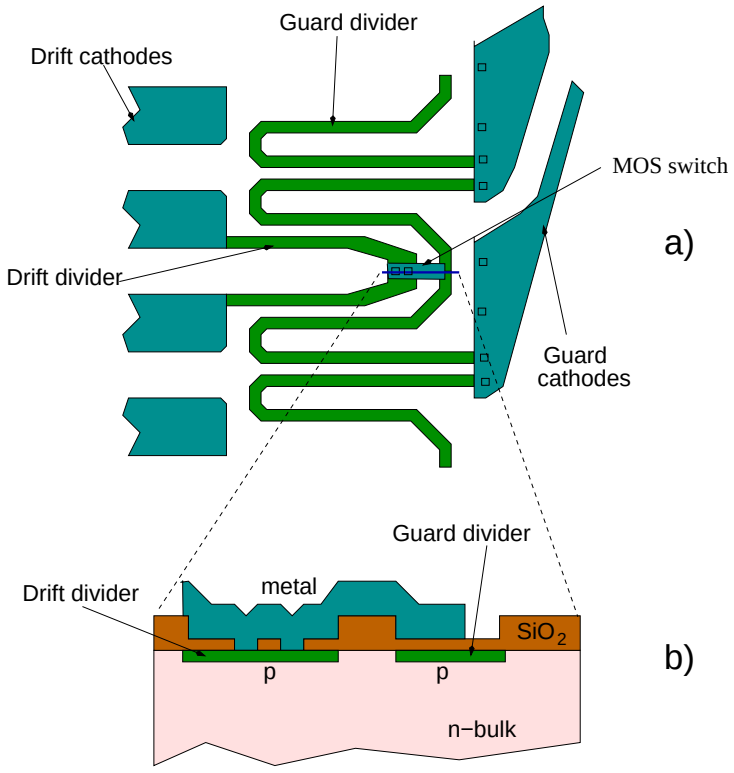

Figure 3: Details of the H.V. integrated divider.

2 Performance of the ALICE SDD integrated divider.

In this paragraph we present the response of the new biasing scheme of the ALICE Silicon Drift Detector to the presence of a localised defect. We carried out the analysis both simulating the structure and performing laboratory measurements.

Firstly, we simulated the behaviour of the MOS switch using ATLAS Semiconductor Device Simulator [18]. We solved both the Poisson's equation and the carrier continuity equation for the 2D-structure shown in figure 3b for various bias conditions. The simulation starts biasing both p^+ implants at $-30V$, in order to reproduce the operation conditions of the ALICE SDD [17]. Then, we vary the potential of one implant, leaving the other unchanged. Applying a more negative potential to the drift resistor, we find that, with a typical value of the fixed oxide charge of $2.0 \times 10^{11} q/cm^2$, a hole current starts to flow from the more positive (guard) resistor to the negative (drift) one at a potential difference of about $0.5V$. Instead, in case of a more positive drift resistor the hole current does not flow till a potential difference of $20V$ between them. It should be pointed out that the laboratory measurements provide a lower value for this potential difference ($U_{p.th.} = 10V$). This happens because, in the region surrounding the MOS switch (where the oxide is not covered with the metal), the voltage needed to activate the hole current flow is lower (see figure 3a).

In order to study the reaction of the entire cathode chain (constituted by the drift and guard cathodes together with their voltage dividers) to the presence of a defect, we used the "Pspice" Simulator program [19]. A fragment of the equivalent circuit, used in the simulations, is presented in figure 4: this part corresponds to the region delimited by the dashed rectangle in figure 2. MOS switches are replaced with Zener diodes having a breakdown voltage equal to $U_{p.th.}$. In this model we include also the leakage current collected by drift and guard cathodes, introducing current sources.

Defects, causing a distortion of the potential distribution, can be grouped in six cases:

1. a bridge between two or more neighbouring drift cathodes,
2. a defect generating high leakage current that enters a drift cathode,
3. an interruption of a drift resistor,
4. a bridge between two or more neighbouring guard cathodes,
5. a defect generating high leakage current that enters a guard cathode,
6. an interruption of a guard resistor.

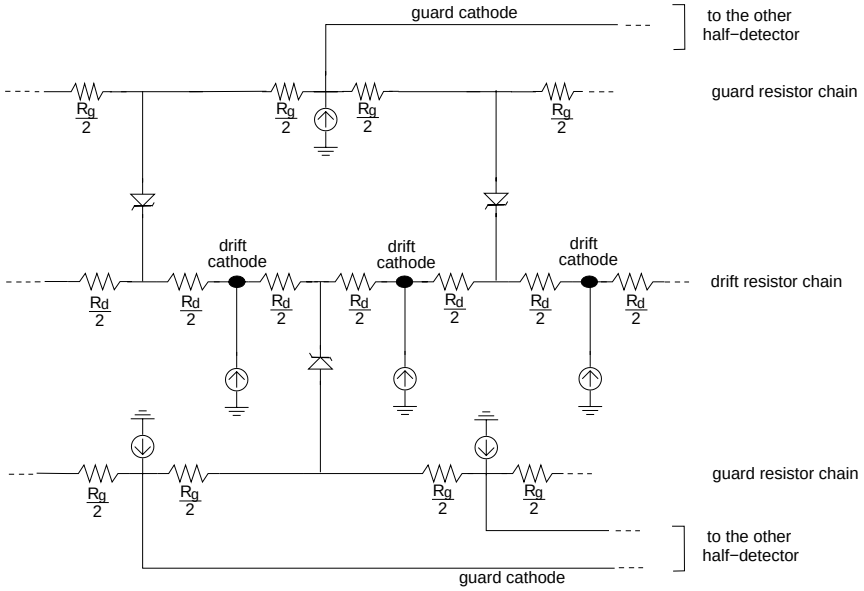

Figure 4: Fragment of the equivalent circuit of the cathode chain.

2.1 Case (1) - Short between cathodes.

The potential distribution in a conventional SDD (equipped with a single voltage divider) in presence of several shorted consecutive cathodes is shown in figure 5. Due to the short,

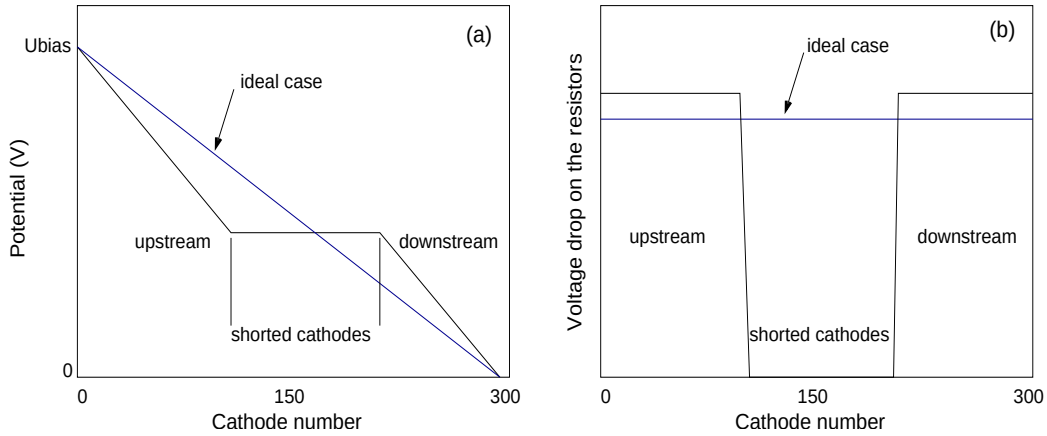

Figure 5: Potential distribution on the drift cathodes (a), and voltage drop between consecutive cathodes (b) in case of few cathodes shorted.

the number of resistors decreases, so, at a given bias voltage, the divider current is higher. As a result, the resistors positioned upstream the defect are more positive than they would be in the ideal case, while the downstream resistors are more negative (figure 5). The upstream and downstream parts of the resulting potential distribution have always equal

slopes. Clearly, on the other half-detector, the potential distribution is the same.
As far as the ALICE SDD is concerned, the situation in more complicated, thus, the Pspice simulator is needed. The simulation of a short can be readily obtained from the circuit in figure 4, connecting together the desired number of drift cathodes. It was experimentally observed that, at maximum, three cathodes may be shorted. Using these values in the simulation, at the nominal bias voltage ($-2400V$), we did not see the transmission of the defect-induced potential deviation to the other half-detector. To evidence it we decided to short 12 consecutive cathodes. Figure 6 shows the progression of the potential distri-

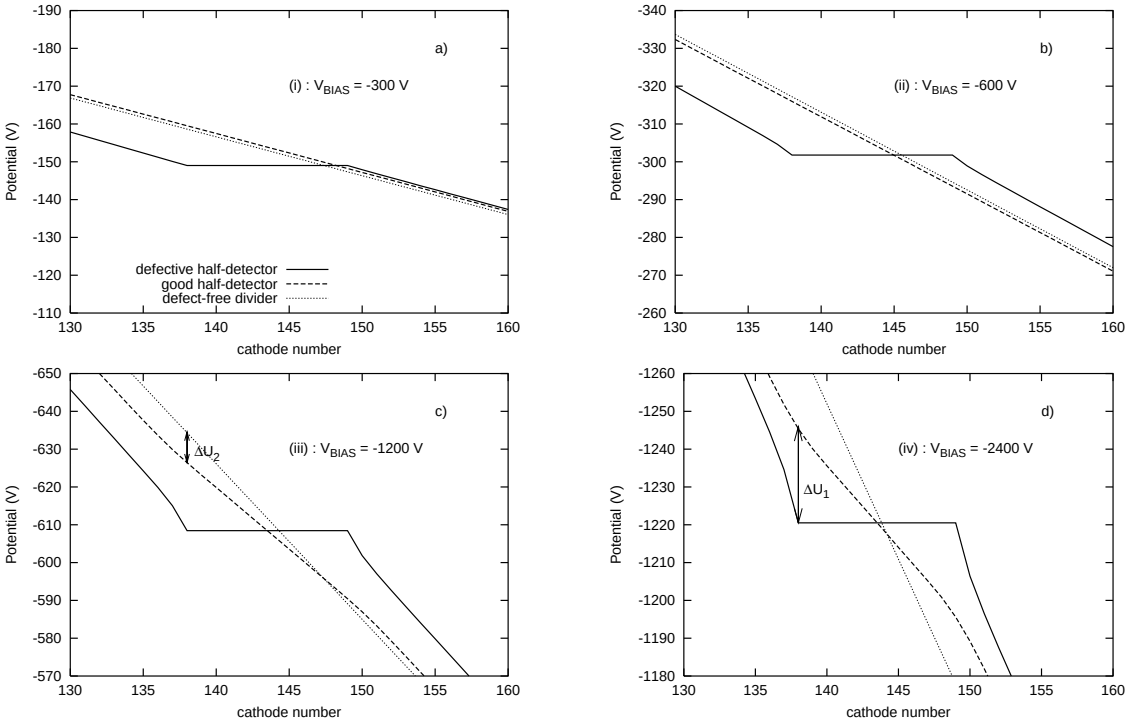

Figure 6: Case (1): Potential distribution as a function of the bias voltage.

bution of the drift cathodes as the bias voltage increases. Even at low bias voltages (see figure 6a), there is a hole current flowing from guard to drift resistors in the downstream part of the defective half-detector. Since the current flowing in the guard dividers is about three times the current of the drift divider of one half, the potential distribution of the downstream part practically coincides with the ideal one. In the upstream part there is no hole current (from drift resistors to corresponding guard resistors), until the potential difference between them does not reach $U_{p.th.}$. Once this value is reached, the drift divider of the defective half and the guard divider are completely bound. Still, the defect is not propagated to the opposite half (figure 6b). This happens only when the other set of MOS structures (between guard dividers and good-half divider) is switched on (figure

6c-d). Figure 7 presents the resume of the progression previously described. The first

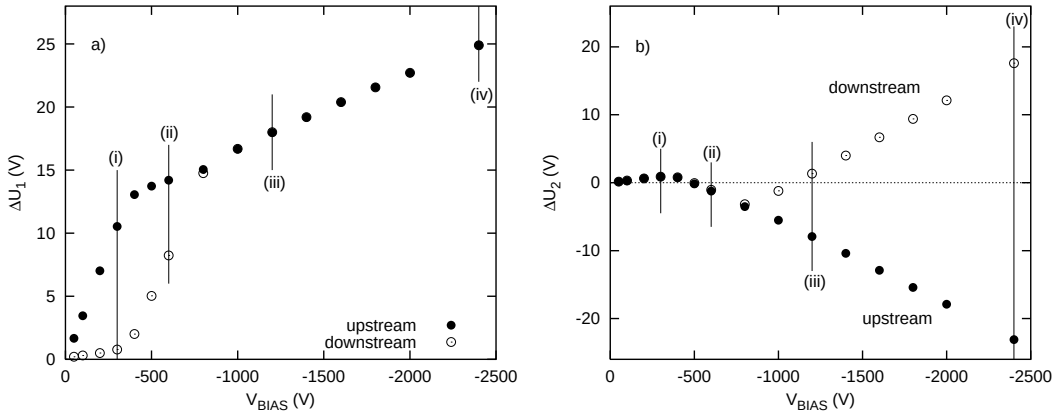

Figure 7: Case(1): Propagation of the potential deviation from one half-detector to the other.

plot shows the potential difference (ΔU_1) between the defective and the good halves in correspondence of the first and the last of the shorted cathodes. The second plot displays the potential difference (ΔU_2) between the above mentioned cathodes of the good half detector and the corresponding cathodes of the defect-free detector. The four bias conditions represented in figure 6 are evidenced with vertical lines. Analysing these plots, we conclude that the propagation of the potential deviation, due to the presence of 12 shorted cathodes, does not occur until a bias voltage of $-800V$.

Instead of drawing the absolute potential, plot 8a shows the voltage drop on each drift resistor as a function of the drift cathode number. The shorts are located in the region where the voltage drop is zero. To verify the simulation results with laboratory measurements, we artificially introduced a bridge between 12 neighbouring drift cathodes of one half-detector by wire-bonding them, and we measured the voltage drop every tenth cathode (figure 9). To compare this data with the simulations, in figure 8b we present the voltage drop in the same format. The measurements show a good agreement with the simulations. We performed several simulations connecting together an increasing number of cathodes. We verified that a defect is not transmitted to the other half, at the nominal bias voltage, until five cathodes are shorted.

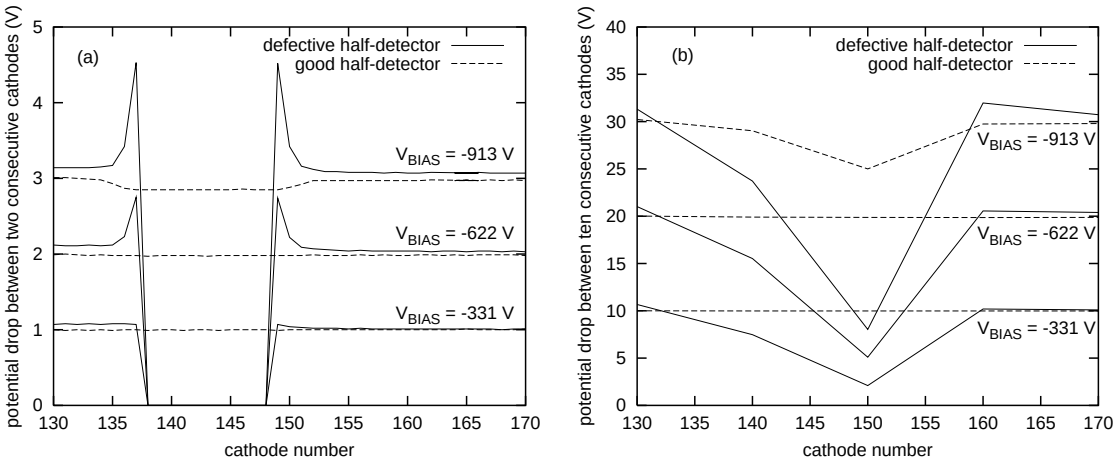

Figure 8: Case (1): voltage drop between two (a) and ten (b) consecutive drift cathodes as a function of the drift cathode number, simulated for both half-detectors.

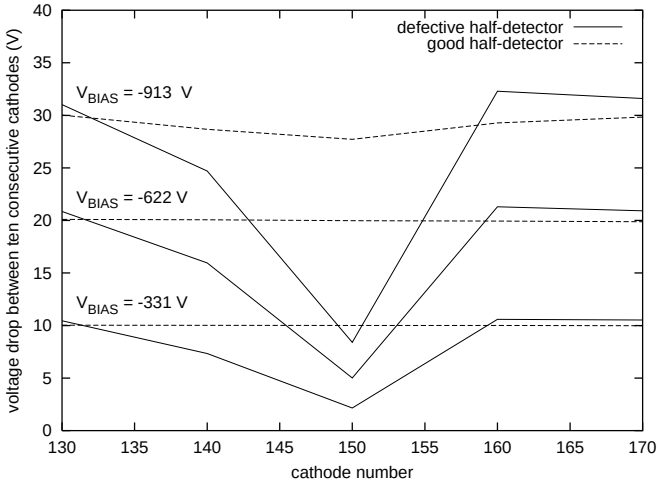

Figure 9: Case (1): measured voltage drop between ten consecutive drift cathodes as a function of the drift cathode number.

2.2 Case (2) - localised high generation centre.

Figure 10 shows the distortion of the potential distribution due to a localised defect generating high current. The hole component of this current enters the cathode chain and sums

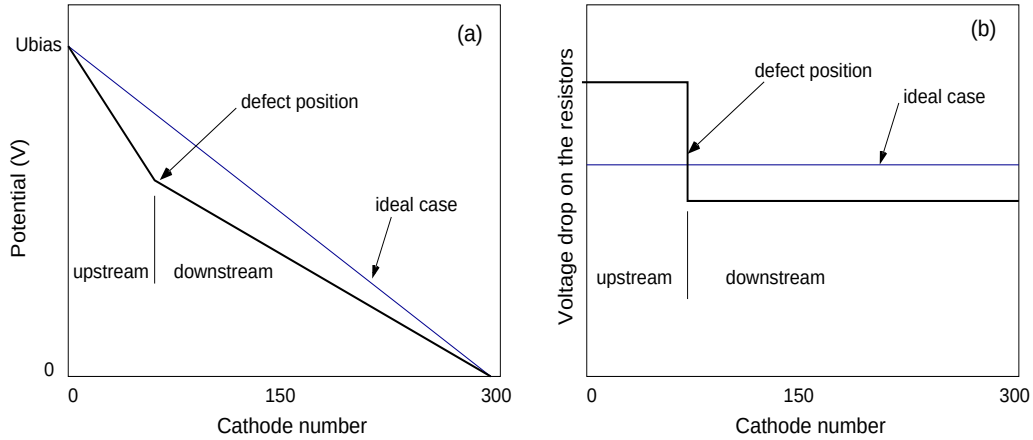

Figure 10: Potential distribution on the drift cathodes (a), and voltage drop between consecutive cathodes (b) in the presence of a defect generating high leakage current.

up to the bias current flowing through the divider. For this reason, the voltage drop on the resistors upstream the defect is higher, and, as a consequence, the slope of the potential distribution is greater [17]. As in case (1), we performed the analysis of the propagation of the defect in a ALICE SDD, using Pspice simulator. To emulate a high generation centre we introduced in the equivalent circuit (fig. 4) a resistance between the defective cathode and ground. Since all drift resistor of the defective half-detector are more positive than the respective guard resistors, there is not a current flow between them until the potential difference does not reach $U_{p.th.}$. Fig. 11 presents the simulated voltage drop on each resistor when the defect is still confined in the 1st half-detector (a1), and when the defect influences also the other half (b1). Plots (a2) and (b2), which represent the voltage drop every tenth cathode, are needed to compare simulation results with measurements. Indeed, as in the simulations, we put a resistance between a drift cathode and ground. The voltage drop distribution measured at a bias voltage of $-1200V$ is shown in figure 12, and it is close to the simulation result. Figure 13 shows the potential difference ΔU_1 between the defective cathode and the corresponding cathode of the opposite half. Again, the measurement is in good agreement with the simulation. The starting point of the plateau ($U_{bias} = -400V$) in the curves indicates the threshold value for ΔU_1 (about $9V$) at which the defect is transmitted to the good half-detector. From this point, the potential distribution of the good half follows the defective one, maintaining a constant ΔU_1. At the onset voltage, the current flowing in the resistance introduced to emulate the defect is

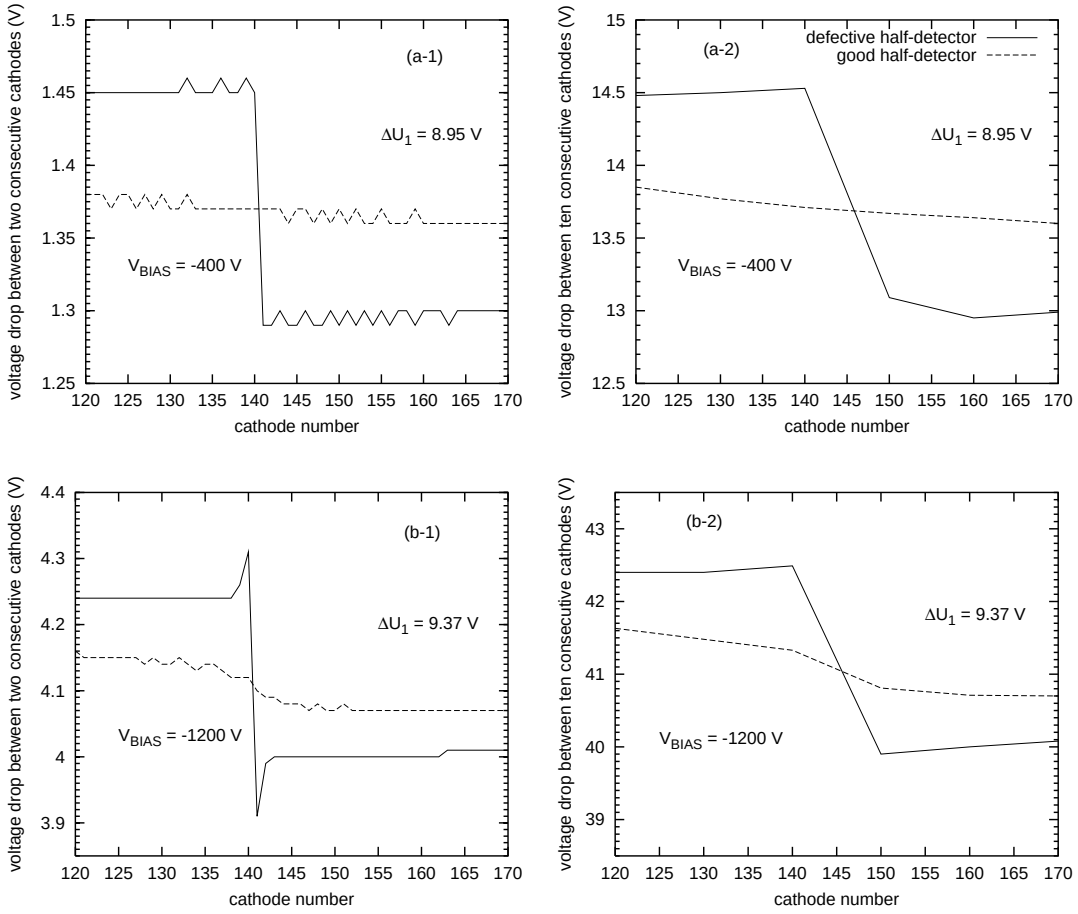

Figure 11: Case (2): Simulated potential drop on each resistor (a1,b1) and between ten consecutive drift cathodes (a2,b2) as a function of the drift cathode number, for both half-detectors.

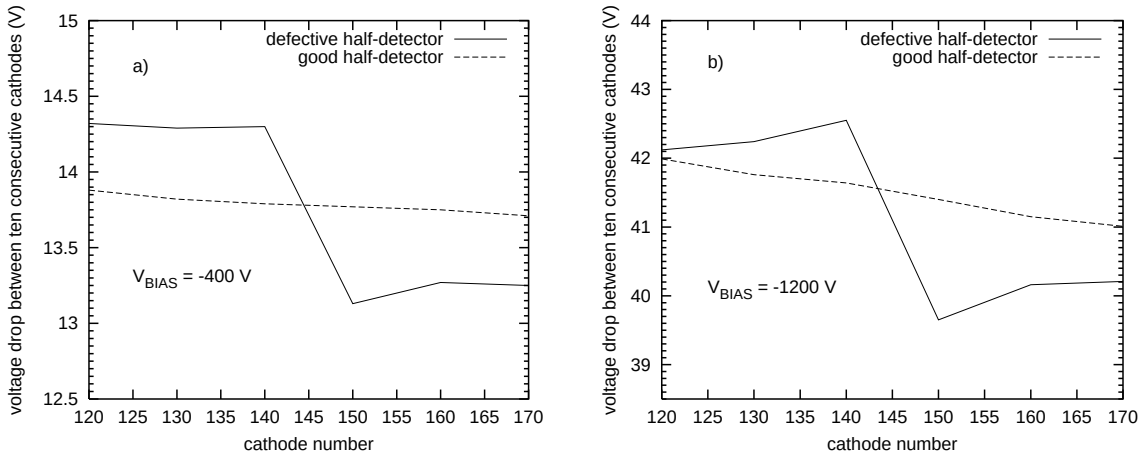

Figure 12: Case (2): measured potential drop between ten consecutive drift cathodes as a function of the drift cathode number.

$1\mu A$. This current grows along with the bias voltage, hence the magnitude of the hypothetical defect would depend on U_{bias}. In reality, the leakage current emitted by a defect does not depend on U_{bias} [17]. So, the critical value of $1\mu A$ found for $U_{bias} = -400V$ is valid for any bias voltage.

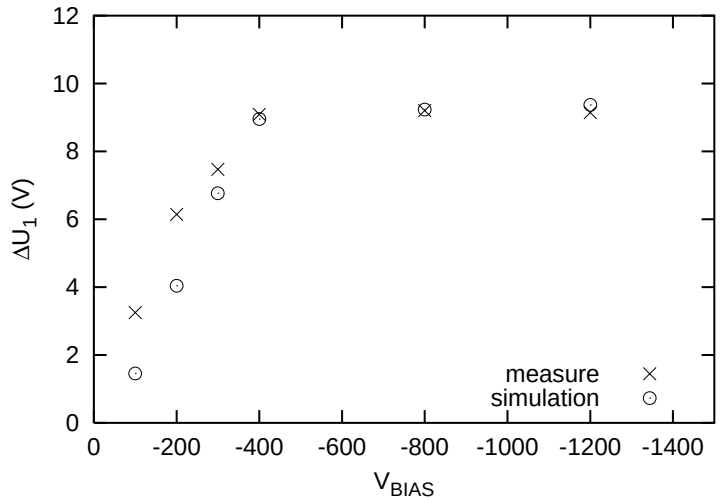

Figure 13: Simulated and measured maximum voltage difference between two halves.

2.3 Cases (3) - Interruption of the drift resistor chain.

The potential distribution in a conventional SDD in presence of an interrupted integrated resistor, is shown in figure 14a. The divider current does not flow through the interrupted resistor until the voltage difference between the edges of the interruption does not reach a critical value $U_{p.th.}$. Anyway, as soon as the two half-detectors are connected via the guards (see figure 1), the current deviates its path through the opposite half-detector. So, at low bias voltages, the voltage drop on the interrupted resistor is twice the nominal one. When the voltage difference between the edges of the interruption reaches $U_{p.th.}$, it remains unchanged and the voltage drop on the interrupted resistor is increased by $U_{p.th.}$ with respect to the nominal value (figure 14b). It is worthwhile noting that the value of $U_{p.th.}$ indicates the width of the interruption: the larger the interruption the higher the punch-through voltage needed to reinstall the hole current through the interrupted resistor.

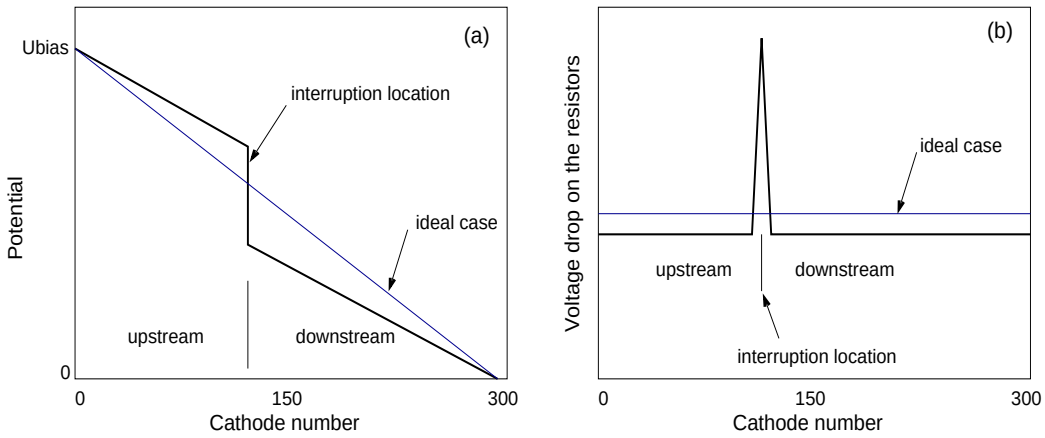

Figure 14: Potential distribution on the drift cathodes (a), and voltage drop between consecutive cathodes in the presence of an interruption on the drift resistor chain.

In case of the ALICE SDD we simulated the interruption of an integrated resistor using a Zener diode. We used different breakdown voltages (from 3 to $21V$) in order to consider various interruption widths. Figure 15 presents the voltage drop distribution for the defective and non-defective half-detector. In this design, there is not a path for the

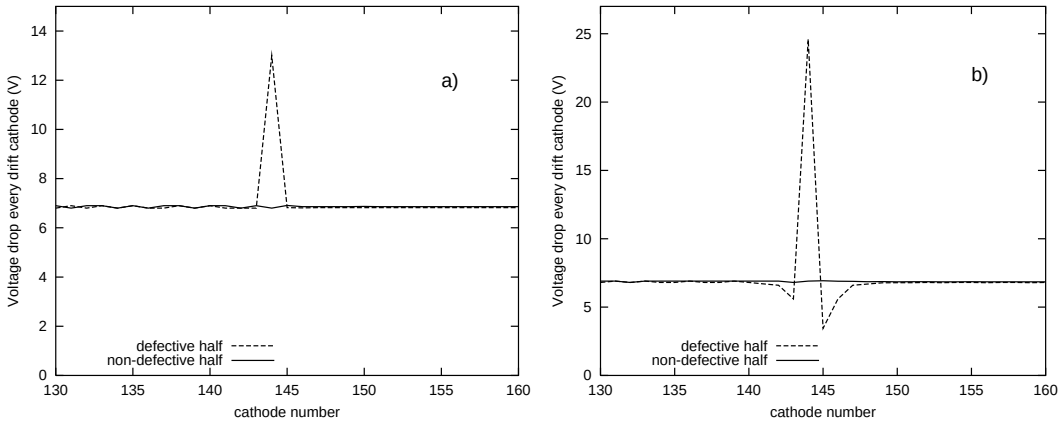

Figure 15: Simulation of the interruption of a drift resistor using two values for $U_{p.th.}$: $9V$ (a), and $21V$ (b).

current through the other half-detector. Similarly to a conventional SDD, only when the voltage difference between the edges of the interruption reaches $U_{p.th.}$, the current is reinstalled through the interrupted resistor. Until the current does not flow, the voltage drop is determined by the MOS-switch connection to the guard resistor chain. For these reasons, the good half is never affected by the interruption on the opposite half.

As an example, figure 16 presents a measurement of the voltage drop of a detector manifesting an interruption. Despite the magnitude of the peak the defect is not transmitted on the good half.

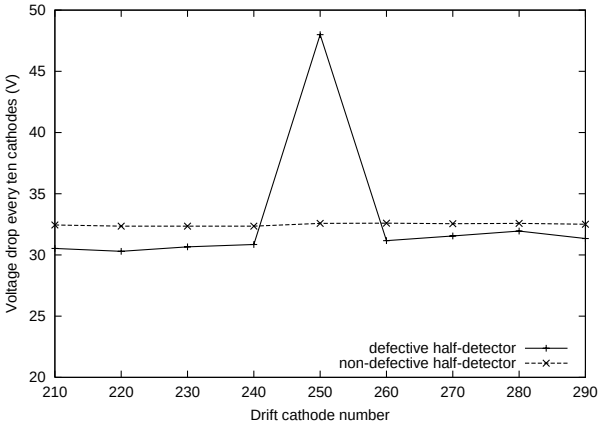

Figure 16: Example of a detector with an interruption (experimental data).

2.4 Cases (4), (5), and (6) - defects in the guard region.

For case (4), in which we consider a bridge between two or more neighbouring guard cathodes, it is enough to repeat the considerations for case (1). Initially, the guard resistors upstream the defect are more positive than the respective drift resistors of both half-detectors. A hole current starts to flow between them even at a low bias voltage, resulting in a prompt propagation of the potential deviation to the drift cathodes of both half-detectors.

In case (5), a defect located in the guard region generates high leakage current that enters the guard divider. Independently from the defect position, any guard resistor is more positive than the respective drift cathodes of both half-detectors. It means that the deviation of the potential distribution on the guard cathodes expands easily to the drift cathodes of both half-detectors.

In case of an interruption on the guard resistor (case (6)), the reaction of the drift divider chain is shown in figure 17. It is interesting to note that the potential deviation is transmitted on the voltage distribution of the drift cathodes in a considerably reduced way.

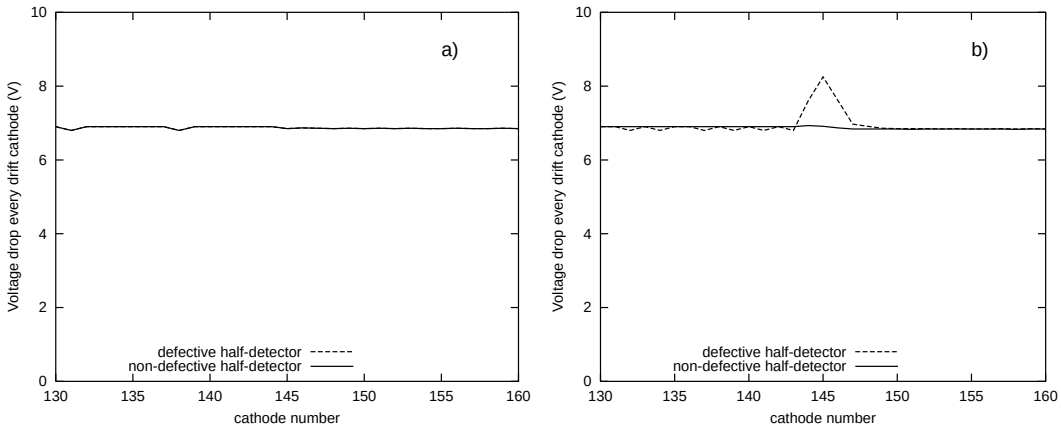

Figure 17: Simulation of the interruption of a guard resistor using two values for $U_{p.th.}$: $9V$ (a), and $21V$ (b).

3 Conclusions.

The main design features of the integrated divider of the ALICE silicon drift detector are presented. The simulation and laboratory tests confirmed that the design allows to attenuate the propagation of the deviation in the potential distribution due to a defect located in a half-detector. In particular, at the ALICE operation voltage, the potential distortion due to a short is not propagated to the non-defective half while the number of interested cathodes is less than five. A high generation centre has to emit more than $1\mu A$ in order to cause a distortion of the potential distribution in both halves. Moreover, an interruption of a drift resistor never affects the potential distribution of the good half.
On the other hand, any type of defect located on the guard cathodes affects promptly the potential distribution on the drift cathodes. It should be considered that a defect generating high leakage current is by far more likely with respect to the other defects. Furthermore, the probability to have it located somewhere on the detector is mainly a geometrical factor, and the guard region occupies only 12% of the total area.

References

[1] ALICE Collaboration, CERN/LHCC 95-71.

[2] ALICE Collaboration, CERN/LHCC, 99/12.

[3] A. Castoldi et al., J. Appl. Phys. 71 (7) (1992) 3593.

[4] E. Gatti et al., Nucl. Instr. and Meth. A 326 (1993) 267.

[5] D. Nouais et al., Nucl. Instr. and Meth. A 461 (2001) 222.

[6] S. Beole' et al., Nucl. Instr. and Meth., in press.

[7] A. Vacchi et al., Nucl. Instr. and Meth. A306 (1991) 187.

[8] G. Gramegna et al., IEEE Trans. on Nuclear Science Vol. 42 (1995) 1497.

[9] S. Beole' et al., Nucl. Instr. and Meth. A360 (1995) 67.

[10] S. Beole' et al., Nucl. Instr. and Meth. A377 (1996) 393.

[11] S. Beole' et al., Il Nuovo Cimento, Vol. 109 A, N. 9 (1996) 1261.

[12] A. Rashevsky et al., Nucl. Instr. and Meth. A409 (1998) 210.

[13] A. Rashevsky et al., Nucl. Instr. and Meth. A461 (2001) 133.

[14] V. Bonvicini et al., Il nuovo Cimento - Vol. 112 A, N. 1-2 (1999) 137.

[15] D. Nouais et al., Nucl. Phys. B (Proc. Suppl.) 78 (1999) 252.

[16] V. Bonvicini et al., Nucl. Instr. and Meth. A 439 (2000) 476.

[17] C. Piemonte, A. Rashevsky, D. Nouais, INFN/TC - 00/04.

[18] SILVACO International, ATLAS User's manual (1998).

[19] Cadence Design Systems, Inc.